Hierarchical Assemblies of Carbon Nanotubes for Ultra-Flexible Li-ion Batteries

By *Shahab Ahmad*, *Davor Copic, Chandramohan George** and *Michael De Volder**

Dr. Shahab Ahmad, Dr. Davor Copic, Dr. Chandramohan George, Dr. Michael De Volder
Institute for Manufacturing, Department of Engineering, 17 Charles Babbage Road,
University of Cambridge, Cambridge, CB3 0FS, United Kingdom
Email: gc495@cam.ac.uk; mfld2@cam.ac.uk

One of the most fascinating paradigm shifts in modern electronics is the fabrication of soft and flexible electronic devices. This development is fuelled by a continuous search for more compact and intuitive consumer electronics,[1] medical implants,[2] and the emergence of the 'Internet of Things'.[3] While considerable progress has been made in the fabrication of flexible and stretchable logics,[4] radio frequency identification (RFID) tags,[5] and displays,[6] the flexible batteries needed to power these devices remain challenging.[7] Existing flexible batteries are often too heavy, bulky, and rigid, and require a radical redesign of the battery architecture to address these issues.[8] Here we show that extremely flexible batteries can be achieved by designing carbon nanotube (CNT) microstructures which decouple the stress induced during bending in the collector electrode from stress in the energy storage material (Fe_2O_3 anodes and $LiNiCoO_2$ cathodes in this work). We found that this battery architecture not only imparts excellent flexibility (bending radii ~ 300 μm), but also high rate (20A/g), cycling stability (over 500 cycles at 1C with capacity retention over 70%).

1

The design of highly flexible batteries requires judicious engineering of the electrodes to mitigate stress concentration and crack formation. Recent, progress towards flexible batteries includes the use of polymer substrates,[9] composite membranes,[10] CNT yarns,[11] paper based electrodes,[12] graphene foams etc.[8,13] However, many of these designs suffer from fast-capacity decay,[14,15] limited flexibility, poor thermal management, and high weight.[8]

In this paper, we propose a design where stress in the electrode is localised in the current collector and decoupled from the electro-active region, which remains unstressed during bending. To achieve this, we populate a flexible current collector with microscale 3D structures which contain the electrochemical active material. In order to remain unstressed as the electrode bends, the base of each active microstructure must be small, and therefore, similar to trees, our microstructures have slender trunk planted in the flexible current collector and a wider crown loaded with electrochemically active nanoparticles. **Figure 1** further illustrates our rationale behind the design of the electrode architecture. Vertically aligned CNT 'Forests' (Fig.1a) have been reported previously as current collectors for high performance non-flexible batteries. CNTs are promising current collectors for batteries because of their electrochemical stability, excellent electrical and thermal conductivity, and large surface area. [8,16-20] However, when CNT forests are bent, they readily crack (Fig. 1e). A solution for this problem is to pattern the electrode material in strips which allows for flexibility in bending along the direction of the strips, however this leads to the same problems when bending in the direction perpendicular to the strips (Fig. 1b). In other words, flexibility in two bending directions requires pillar-like geometries, but even then, the ratio between the bending radius and the pillar base should remain sufficiently high to avoid stress at the interface between the pillars and current collector (see Fig. 1c). Therefore, this work focusses on microcones as a novel geometry, combining a slander base for stress reduction and a wide crown for particle loading, as shown in Fig. 1d. A further motivation for using

cones instead of pillars is that CNT pillars form unpredicable wrinkles dusing the capillary aggregation steps used in our battery fabrication process (see further).[21] SEM images of plain CNT forests bent to a radius of 3 mm already show cracks (Fig. 1e), while micro-cone electrodes bent to radii as small as 300 μm remain intact (Fig. 1f).

Figure 2 depicts the electrode fabrication process, which starts by lithographically patterning catalyst particles into rings from which CNTs are grown by thermal chemical vapour deposition (CVD; see methods and Fig. 2a). The CVD process results in the formation of micro-cylinders that each consists of thousands of vertically aligned CNTs (Fig. 2b). Next, these cylinders are transformed into cones using elasto-capillary aggregation.[21-23] (Fig. 2c) Shortly, this process uses capillary forces to pull the CNTs into a close packing, which results in an overall compaction of the CNT cylinders into cones (Fig. 2d and Fig. S1 of the Supporting information).[22] The cones are then transferred by contact printing[24] to a flexible conductive film (Fig. 2e) consisting of polyvinydlene difluoride (PVDF), double wall CNTs and Phenyl-C61-butyric acid methyl ester (PCBM) in a ratio (90:5:5) which are thoroughly mixed using a planetary ball mill and casted in ~15 μm thick films, see methods for details. The flexible film is referred to as PCP (**P**VDF, **C**NT and **P**CBM) in what follows. A top SEM view (Fig. 2i) of the film shows that the CNTs bundle into rafts similar to previous reports,[25] and cross-sectional SEM images (Fig. S2 of the Supporting information) show a uniform spread of material through the film thickness. Interestingly, our PCP film (1cm^2) is found to be ~20 times lighter in weight on comparison with standard Cu-foil electrodes (MTI corporation Code EQ-bccf-25μ, Fig. S3 of the Supporting information). Fig 2f,j show that the CNT cones can be transferred with yields close to 100%. Further, it is important to note that most of the catalyst particles remain attached to the silicon substrate after the CNT transfer printing process, and therefore the Si-substrate can be recycled to synthesise new CNT cones. With our current process the catalyst can be re-grown about 4 times before losing its activity.[26]

Finally, the electrodes are decorated with Fe_2O_3 nanocrystals (~10 nm diameter, Fig.2g, S5 of the Supporting information) by dropcasting a carefully weighed hexane - Fe_2O_3 suspension. The iron oxide nanocrystals are synthesized by a colloidal method which involves decomposing iron pentacarbonyl in octadecene in the presence of oleylamine (see methods and Supporting information).[27] Iron oxide is chosen as the anode material because of its high theoretical capacity (~1000 mAh/g), low cost, environmental friendliness and abundancy.[28,29] In addition, the conversion reactions that take place between Fe_2O_3 and Li during charge/discharge cycles require good electrical contact which is provided by our unique CNT microcone architecture. SEM images of transferred cones on PCP film, loaded with Fe_2O_3 nanoparticles (~0.5-1 mg) are shown in Fig. 2k,l and Fig. S4 of the Supporting information.

The electrodes are packaged, using both rigid coin-cells (2032) with Li metal cathodes (see methods) and flexible laminated packages using cathodes made using the same CNT cones but decorated using commercial, lithium nickel cobalt oxide powder (LNCO, Sigma-Aldrich 760986) because Li metal has a limited flexibility.[8] In a first series of tests we use the coin cells to compare our hierarchical microcones decorated with Fe_2O_3 to conventional electrodes fabricated by mixing the same Fe_2O_3 nanoparticles with the CNT based PCP film. **Figure 3a** shows that the charge/discharge curves of both electrodes have a sloping plateau at ~1.8 V corresponding to the first-step lithiation of Fe_2O_3. This becomes more defined at ~1.2 V with the onset of conversion reaction and at voltages below 1.0 V, the sharp increase of current can be attributed to a full conversion coupled with the formation of a solid electrolyte interface (SEI).[30] These processes can also be seen in the cyclic voltammogram (Fig. 3a inset) with a gradual lithiation/delithtaion of Fe_2O_3 at 1.8 V, 1.2 V, 0.5V and 2.0 V, in accordance to typical reports on conversion of Fe_2O_3 (i.e. $Fe_2O_3+6Li\rightarrow2Fe+3Li_2O$).[29,31,32] The peak at 0.7-

1.0 V corresponding to Li^+ ion insertion into Fe_2O_3 is more pronounced in the CNT-cone electrodes, suggesting a facile lithiation reaction.

The initial capacity of the CNT cones is ~1000 mAh/g at 0.5 C while the conventional electrodes yielded only ~800 mAh/g (Fig. 3a discharge curves), but in the subsequent cycles the conventional electrode loses more than half of the initial capacity (Fig. 3b), while the CNT cone electrodes remarkably retain more than 70 % of their initial capacity. At high current densities (rates), CNT cone electrodes clearly outperform the capacity and retention of the conventional reference electrodes (Fig. 3b). For instance, the capacity of conventional electrodes quickly fades and reaches values close to 0 mAh/g at a rate of 7 C (Fig. 3b) which indicates poor electrochemical activities while the microcone electrodes maintain more than 300 mAh/g under the same conditions. Such drop in performance of conventional electrodes where the metal oxide is blended in a polymer binder was also reported previously.[33] In comparison, the CNT cone electrodes still yielded appreciable capacity at 10, 15, and 20 C (Fig. 3c), and despite these harsh high rate tests, the electrodes still exhibited sustained capacities 600-700 mAh/g when the rate was reduced to 0.5 C. We initially observed a difference in charge and discharge capacity after reverting from high to low rate which might be due to the binder free nature of our electrode architecture and the thick deposition of active particles built up of multiple layers. The cone architecture therefore not only imparts excellent flexibility, but also enhances battery performance substantially. Because the cones bring the active material outside of the binder, the electrochemical reactions take place at the surface of the CNT cones which protects the collector electrode from the deleterious side reactions between active materials (Fe, Li_2O and Fe_2O_3) and binder molecules which can lead to large internal resistance. Furthermore, the developed CNT cones are able to accommodate the drastic volume change[34] taking place during conversion reactions, and ensure good contact to the active material resulting in the observed higher charge retention, also compared to other recently published CNTs-metal oxide electrodes.[33,35,36] Finally, the cone electrodes were

cycled 500 times at 1 C with no appreciable change in the capacity as shown in Fig. 3d, and we further compare the performance of our battery to those based on CNT forests previously reported in supporting information table S1.

Finally, we have constructed flexible full cells with both CNT cone anodes and cathodes, as depicted in the schematics of **Figure 4a**. The former is coated with Fe_2O_3 as discussed above, and the cathode with commercial LNCO powder (see methods). Fig 4b shows the charge/discharge curves from the full cell. The full cells were folded multiple times and then tested in flat state, they operate around 3.3V with a sloping plateau between 4.0-2.0V and the capacity was stabilised after the second cycle (for LNCO), and delivers a reversible capacity of ~120 mAh/g at 2C (Fig. 4b). Figure S6 shows further cycling data of the battery while it is being bent and released for 15 cycles. These batteries were connected to a white light emitting diode (LED, 3V) and flexed to radii of about 3 mm while powering the LED as illustrated in Fig. 4c. The bending radius is currently limited by the packaging rather than the electrodes themselves (more information in supporting information). Finally, complex electrode architectures are often not able to survive the harsh battery cycling conditions. Therefore, we opened our flexible cells after 1000 cycles which corresponds to the lifetime of the battery to image the CNT cones. Figure 4e reveals that the overall cone morphology is well maintained, similar to as fabricated CNT cones shown in Figure 4d. We believe this is because the cones are well anchored in the collector electrode, and because capillary aggregated CNT structures are substantially more resilient than as-grown forests.[21]

In conclusion, this paper presents a new electrode architecture which consists of hierarchical cone shaped CNT structures with a slender trunk embedded in a flexible light weight collector electrode and a wide crown that is loaded with nanocrystals for energy storage. This architecture allows the electrodes to be folded to very small radii without inducing stress in the active material network. These unique electrodes not only alleviate stress, but also bring the active particles outside of the binder which dramatically enhances the performance of the

conversion reactions. This results in batteries that are extremely flexible (300μm radii) and at the same time offer excellent rates (as high as 20A/g), and cyclability (over 500 cycles at 1C with capacity retention >70%).

Experimental Section

Lithography: Clean (100) silicon wafers are first de-hydrated at 200 °C., and coated with an adhesion promoter (Ti-prime). Then AZ 4533 photoresist is spin coated (3000 rpm, 30 s) and pre-baked at 115 °C for 2 mins on hot plate, and exposed. The patterns are developed in diluted AZ 351B (1:4 DI water, 3 mins), followed by rinsing in DI water and blow-drying.

CNT growth. E-beam evaporation is used to deposit a 10 nm Al_2O_3 and 1 nm Fe catalyst film. The Si-wafers are then diced and the catalyst is patterned by lift-off. Next, CNT forests are grown in cylindrical structures by thermal CVD in a horizontal tube furnace at atmospheric pressure, with flows of 100/400/100 sccm $C_2H_4/H_2/He$, at 800 °C. The CNTs are rapidly cooled in the growth atmosphere before purging the CVD chamber with Helium.

Densification, PCP film fabrication and transfer printing: The cylindrical CNT microstructures are converted into elongated cone-like structures by a capillary forming process reported previously[22]. These CNT microcones are transferred onto the flexible PCP film, which is fabricated as follows: 15 mg of methanofullerene phenyl C61 butyric acid methyl ester (PCBM) is dissolved in 3 ml dimethylformamide (DMF) and ultra-sonicated for 1 hour. 15 mg double wall carbon nanotubes (DWCNTs -Nanocyl NC2000) are added to the PCBM solution and ultrasonicated for 30 minutes. A solution of polyvinylidene fluoride (PVDF) (300 mg in 3 ml DMF) is added as binder to the CNT-PCBM solution and stirred. Finally the PVDF-CNT-PCBM suspension is ball milled (planetary) in grinding jar (25 ml) with single metal ball for 2 hours with an interval of 30 s after every 2 minutes. The ball-milled PCP suspension is drop-casted over clean soda-lime glass slide. The temperature of the

glass substrate is increased to 60 °C to dry the film and is then raised to 175 °C to soften the PVDF. The densified CNT cones are then transferred on the PCP film by micro-contact printing[24].

Nanocrystal synthesis and coating: Iron oxide (Fe_2O_3) nanocrystals are synthesised by a colloidal method which involves decomposing iron pentacarbonyl ($Fe(CO)_5$ ~1-2 mL) in octadecene (~20 mL) in the presence of oleylamine and oleic acid mixture (~1.5 mL) as reported previously[27]. More synthesis details are provided in supporting information, along with an XRD scan (Fig. S5 of the Supporting information). Purified iron oxide nanoparticles, suspended in hexane, were drop casted onto the CNT microstructures at 40°C. The substrate is left in air for few minutes to completely evaporate the solvent. The PCP film with CNT microstructures is then peeled-off from the glass substrate. The flexible electrode was tested in half cells with 2032 coin type casings with pure Li metal as reference and counter electrode, and was separated by a layer of polypropylene (PP). 1 M $LiPF_6$ served as the electrolyte. The battery fabrication and equilibration of cells were carried out in an argon (Ar) filled glovebox at room temperature. The full cells were fabricated by drop casting Fe_2O_3 nanoparticles and commercial LNCO powder (from Aldrich - lithium cobalt nickel oxide powder< 0.5 μm 760986) on CNT cone electrodes. These were separated by a polypropylene layer or Whatman borosilicate paper soaked with 1 M $LiPF_6$ as electrolyte, and the pack was laminated.

Conventional electrode fabrication: For comparison, conventional flexible electrodes are fabricated by adding 200 μl of Fe_2O_3 nanoparticles (in hexane or chloroform) to 1ml of pre-synthesised and ball-milled PCP suspension (DMF). The composite suspension was sonicated and then stirred for 1hour each before dropcasting into film and packaging the battery in the same way as described above.

Supporting Information

Supporting Information is available online from Wiley InterScience or from the author.

Received: ((will be filled in by the editorial staff))
Revised: ((will be filled in by the editorial staff))
Published online: ((will be filled in by the editorial staff))

[1]   T. Someya, *Nat. Mater.* **2010**, *9*, 879.

[2]   R. C. Webb, A. P. Bonifas, A. Behnaz, Y. Zhang, K. J. Yu, H. Cheng, M. Shi, Z. Bian, Z. Liu, Y.-S. Kim, W.-H. Yeo, J. S. Park, J. Song, Y. Li, Y. Huang, A. M. Gorbach, J. A. Rogers, *Nat. Mater.* **2013**, *12*, 938.

[3]   Y. Zhan, Y. Mei, L. Zheng, *J. Mater. Chem. C* **2014**, *2*, 1220.

[4]   J. A. Fan, W.-H. Yeo, Y. Su, Y. Hattori, W. Lee, S.-Y. Jung, Y. Zhang, Z. Liu, H. Cheng, L. Falgout, M. Bajema, T. Coleman, D. Gregoire, R. J. Larsen, Y. Huang, J. A. Rogers, *Nat. Commun.* **2014**, *5*, 3266.

[5]   J. A. Rogers, T. Someya, Y. Huang, *Science* **2010**, *327*, 1603.

[6]   J. A. Rogers, *Science (80-.).* **2001**, *291*, 1502.

[7]   H. Nishide, K. Oyaizu, *Science* **2008**, *319*, 737.

[8]   X. Wang, X. Lu, B. Liu, D. Chen, Y. Tong, G. Shen, *Adv. Mater.* **2014**, *26*, 4763.

[9]   M.S. Jung, J.H. Seo, M.-W. Moon, J. W. Choi, Y.C. Joo, I.-S. Choi, *Adv. Energy Mater.* **2015**, *5*, 1400611.

[10]   N. B. Aetukuri, S. Kitajima, E. Jung, L. E. Thompson, K. Virwani, M.-L. Reich, M.

Kunze, M. Schneider, W. Schmidbauer, W. W. Wilcke, D. S. Bethune, J. C. Scott, R. D.

Miller, H.-C. Kim, *Adv. Energy Mater.* **2015**, *5*, 1500265.

[11]   J. Ren, Y. Zhang, W. Bai, X. Chen, Z. Zhang, X. Fang, W. Weng, Y. Wang, H. Peng,

Angew. Chemie Int. Ed. **2014**, *53*, 7864.

[12]   L. Hu, H. Wu, F. La Mantia, Y. Yang, Y. Cui, *ACS Nano* **2010**, *4*, 5843.

[13]   N. Li, Z. Chen, W. Ren, F. Li, H.-M. Cheng, *Proc. Natl. Acad. Sci.* **2012**, *109*, 17360.

[14]   V. L. Pushparaj, M. M. Shaijumon, A. Kumar, S. Murugesan, L. Ci, R. Vajtai, R. J.

Linhardt, O. Nalamasu, P. M. Ajayan, *Proc. Natl. Acad. Sci. U. S. A.* **2007**, *104*, 13574.

[15]   B. J. Landi, M. J. Ganter, C. M. Schauerman, C. D. Cress, R. P. Raffaelle, *J. Phys.*

Chem. C **2008**, *112*, 7509.

[16]   S. H. Choi, J.-H. Lee, Y. C. Kang, *ACS Nano* **2015**, *9*, 10173.

[17]   J. Liu, K. Song, P. A. van Aken, J. Maier, Y. Yu, *Nano Lett.* **2014**, *14*, 2597.

[18]   X. Jia, Y. Kan, X. Zhu, G. Ning, Y. Lu, F. Wei, *Nano Energy* **2014**, *10*, 344.

[19]   M. De Volder, S. H. Tawfick, R. H. Baughman, A. J. Hart, *Science* **2013**, *339*, 535.

[20]   J. Chen, Y. Liu, A. I. Minett, C. Lynam, J. Wang, G. G. Wallace, *Chem. Mater.* **2007**,

19, 3595.

[21]   a) M. De Volder, S. J. Park, S. H. Tawfick, D. O. Vidaud, A. J. Hart, *J.*

Micromechanics Microengineering **2011**, *21*, 045033; b) M. De Volder, A. J. Hart,

Angew. Chemie - Int. Ed. **2013**, *52*, 2412.

[22]   M. De Volder, S. H. Tawfick, S. J. Park, D. Copic, Z. Zhao, W. Lu, A. J. Hart, *Adv.*

Mater. **2010**, *22*, 4384.

[23]   Y. Hayamizu, T. Yamada, K. Mizuno, R. C. Davis, D. N. Futaba, M. Yumura, K. Hata,

Nat. Nanotechnol. **2008**, *3*, 289.

[24]   Z. Rong, Y. Zhou, B. Chen, J. Robertson, W. Federle, S. Hofmann, U. Steiner, P.

Goldberg-Oppenheimer, *Adv. Mater.* **2014**, *26*, 1456.

[25]   J. Wu, L. Jiao, A. Antaris, C. L. Choi, L. Xie, Y. Wu, S. Diao, C. Chen, Y. Chen, H. Dai, *Small* **2013**, *9*, 4142.

[26]   M. De Volder, S. Tawfick, S. J. Park, A. J. Hart, *ACS Nano* **2011**, *5*, 7310.

[27]   C. George, D. Dorfs, G. Bertoni, A. Falqui, A. Genovese, T. Pellegrino, A. Roig, A. Quarta, R. Comparelli, M. L. Curri, R. Cingolani, L. Manna, *J. Am. Chem. Soc.* **2011**, *133*, 2205.

[28]   J. S. Chen, T. Zhu, X. H. Yang, H. G. Yang, X. W. Lou, *J. Am. Chem. Soc.* **2010**, *132*, 13162.

[29]   M. V. Reddy, T. Yu, C. H. Sow, Z. X. Shen, C. T. Lim, G. V. Subba Rao, B. V. R. Chowdari, *Adv. Funct. Mater.* **2007**, *17*, 2792.

[30]   A. Paolella, R. Brescia, M. Prato, M. Povia, S. Marras, L. De Trizio, A. Falqui, L. Manna, C. George, *ACS Appl. Mater. Interfaces* **2013**, *5*, 2745.

[31]   Q. Su, D. Xie, J. Zhang, G. Du, B. Xu, *ACS Nano* **2013**, *7*, 9115.

[32]   B. Tian, J. Światowska, V. Maurice, S. Zanna, A. Seyeux, L. H. Klein, P. Marcus, *J. Phys. Chem. C* **2013**, *117*, 21651.

[33]   A. Goyal, A. L. M. Reddy, P. M. Ajayan, *Small* **2011**, *7*, 1709.

[34]   C. Kim, S. Choi, S. Yoo, D. Kwon, S. Ko, J.-M. Kim, S.-Y. Lee, I.D. Kim, S. Park, *Nanoscale* **2015**, *7*, 11286.

[35]   J. Lee, C. Jo, B. Park, W. Hwang, H. I. Lee, S. Yoon, J. Lee, *Nanoscale* **2014**, *6*, 10147.

[36]   G. Zhou, D.W. Wang, P.X. Hou, W. Li, N. Li, C. Liu, F. Li, H.-M. Cheng, *J. Mater. Chem.* **2012**, *22*, 17942.
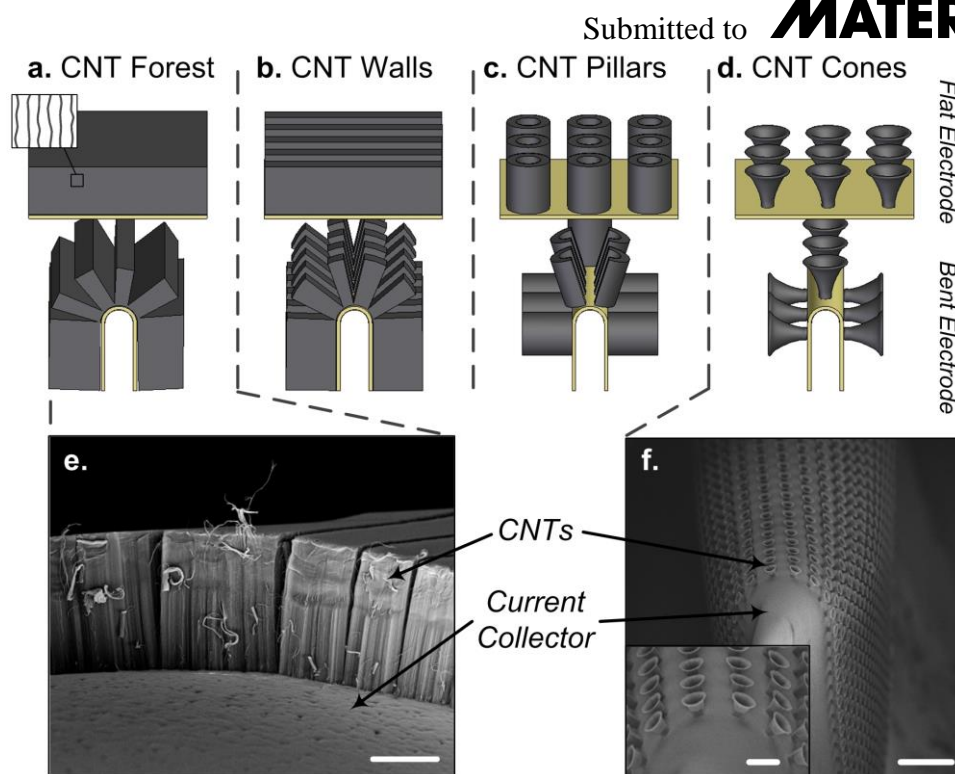
Figure 1. Electrode architectures (top) and their deformation when bent (bottom). (a) Unpatterned CNT forest on flat (top) and bent (bottom) substrate. (b) CNT forests patterned in strips on flat (top) and bent (bottom) substrate. (c) CNT forests patterned in cylinders on flat (top) and bent (bottom) substrate. (d) CNT cones on flat and bent substrate. (e) Scanning electronic microscopic (SEM) image showing cracks in a CNT forest bent to a radius of 3 mm. Scale bar, 40 μm. (f) SEM image of a bent CNT cone electrode. Scale bar, 400 μm. Inset shows the magnified view SEM image. Scale bar, 100 μm.
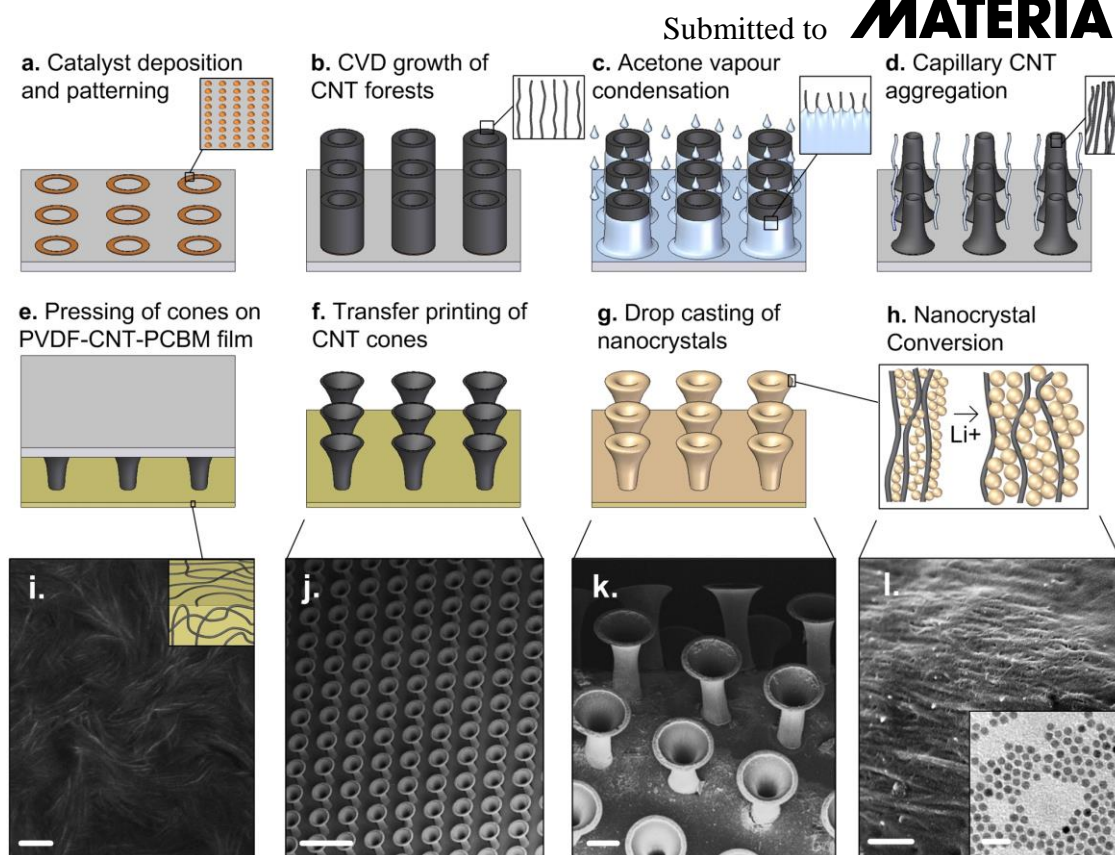
Figure 2. Fabrication process schematics and characterizations. (a) Photo-lithographically patterned Fe catalyst film deposited by e-beam evaporation (inset shows formation of nano-structured Fe islands after hydrogen annealing at 800 °C). (b) CNT cylinders grown by CVD. (c) Capillary aggregation by acetone vapours. (d) Aggregated CNT-cones. (e) Transfer-printing of CNT cones on the flexible PCP film. (f) Transferred CNT cones PCP film. (g) Dropcasting of Fe_2O_3 nanocrystals. (h) Close-up view of the Fe_2O_3 coating. (i) Top view SEM image of flexible CNT-polymer PCP film. Scale bar, 200 nm. (j) SEM image of transferred CNT cone structure assemblies. Scale bar 200 μm. (k) SEM image of bent electrode coated with Fe_2O_3 nanocrystals. Scale bar, 40 μm. (l) SEM image of the Fe_2O_3 nanocrystals coating. Scale bar, 500 nm. Inset shows a transmission electron microscope image of the iron oxide nanocrystals. Scale bar, 20 nm.
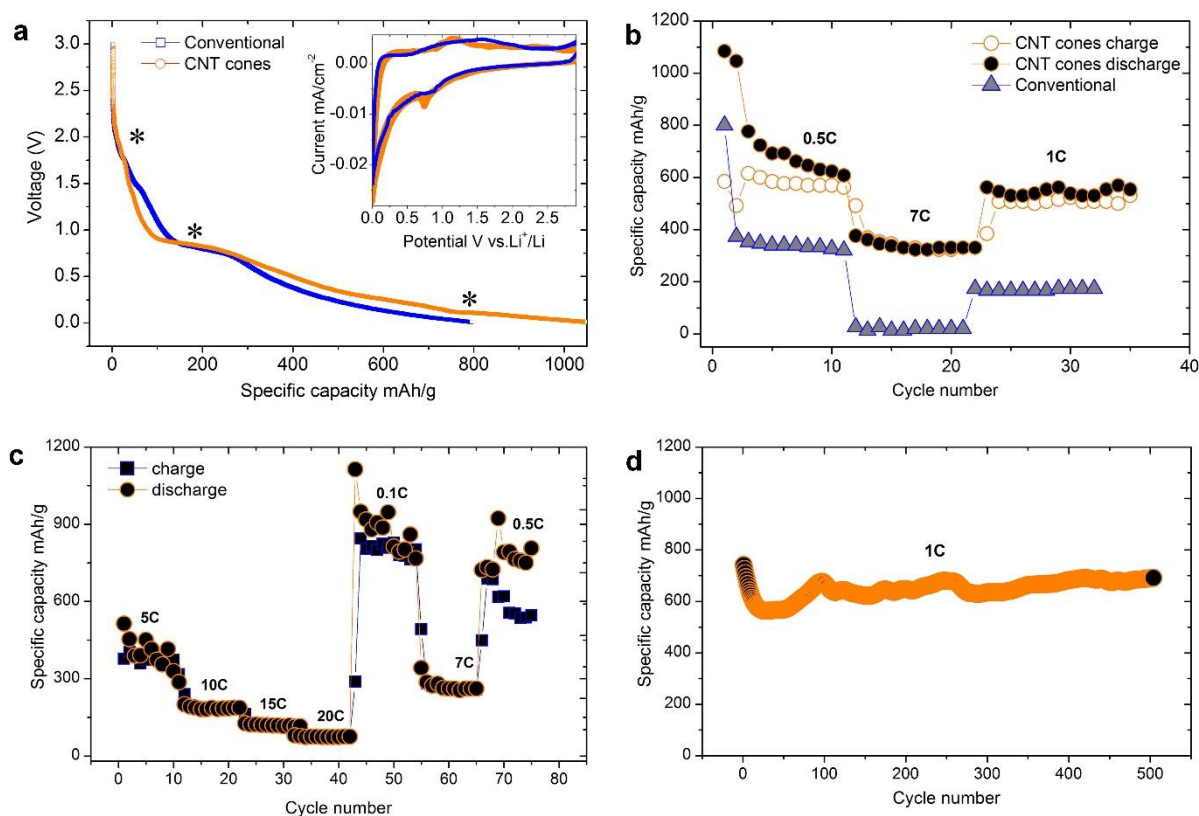
Figure 3. Electrochemical performance comparison of CNT cones-Fe_2O_3 and conventional electrodes with Fe_2O_3. (a) Discharge cycles, and cyclic voltammetry at 0.5 mV/s (inset). (b) Cycling performance of both microcone and conventional electrodes. (c) High rate performance of the CNT cone electrodes. (d) Extended life-time testing of the CNT cone electrodes at 1C rate for 500 cycles.
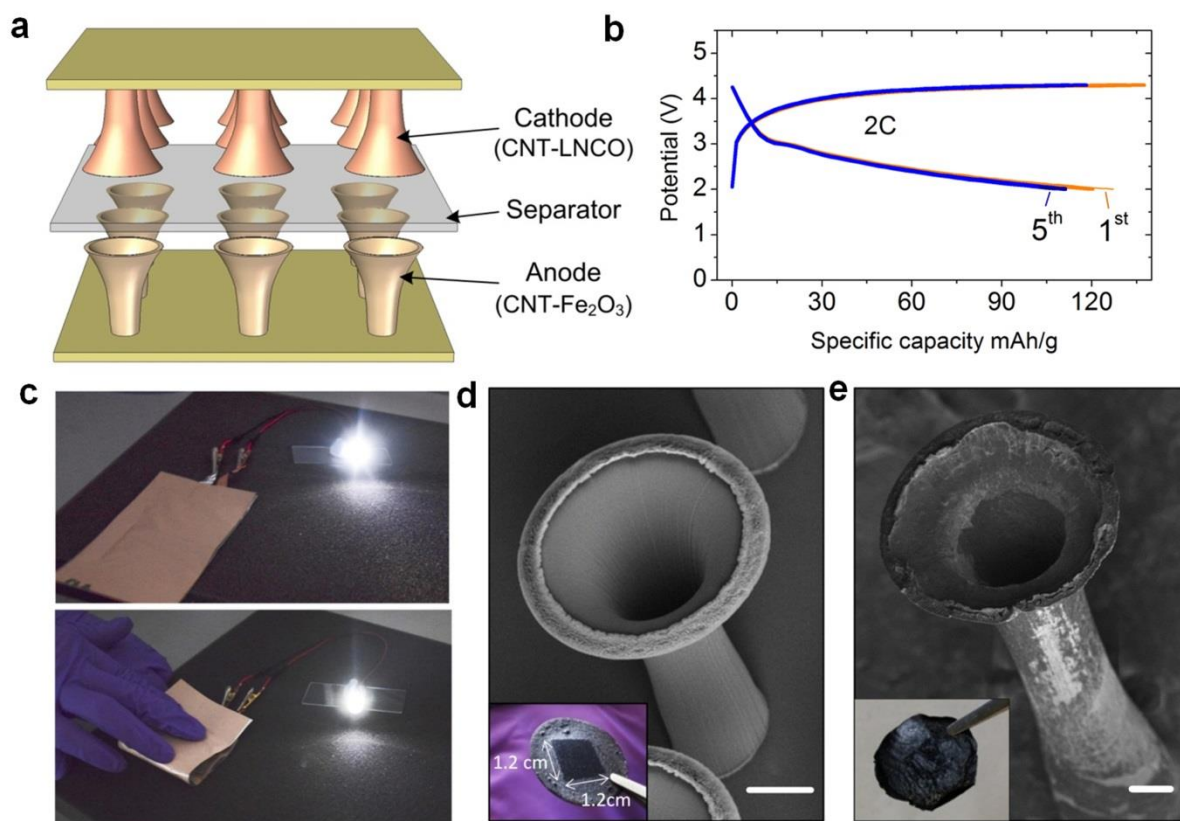
Figure 4. Full flexible cell fabrication and characterizations. (a) Schematic representation of the full cell with a CNT cone anode and cathode. (b) Charge/discharge curves of full cell: iron oxide-CNT cones and LNCO-CNT cones at 2C (first cycle orange - fifth cycle blue). (c) Flexible CNT cone battery connected to a 3V white light LED. (d) SEM image of CNT cone, taken at 35° tilt angle, before testing in full cell. Inset shows 1.2 cm x 1.2 cm area coverage of transferred CNT cones on PCP film. Scale bar 20 μm. (e) SEM image of CNT cone, taken at 40° tilt angle, and picture of the electrode (inset) after 1000 charging and discharging cycles and repeated bending of the electrode. Scale bar, 10 μm.

# Supporting Information

Iron-Oxide Nano crystal synthesis:

Iron metal oxide nanocrystals (Fe_2O_3) have been synthesised by a colloidal method which involves decomposing iron pentacarbonyl ($Fe(CO_5)$) in octadecene in the presence of oleylamine. In a typical synthesis, to 20 ml of octadecene in a three necked flask added 2 ml of oleylamine and heated to 120 °C for 5 min. Then, 5 ml of Iron pentacarbonyl was injected and the temperature was raised to 180-270 °C for 1-3 hr. The resulted dark brown solution was blown air for oxidizing the nanocrystals. The nanocrystals were washed several times (3-5) with a mixture of 1:1 v/v ethanol/toluene mixture and finally dispersed in pure hexane.

Materials:

The following chemicals were purchased from Sigma-Aldrich: iron pentacarbonyl [$Fe(CO)_5$] (99.99 %), oleylamine (70 %), 1-octadecene (ODE, 90 %) and oleic acid (90 %). Electrochemical grade propylene carbonate, ethylene carbonate, diethyl carbonate, N-methyl-2-pyrrolidone, polyvinylidene fluoride (PVDF), and Li metal foils were purchased from Sigma-Aldrich. Industry standard DWCNTs were purchased from Nanocyl (NC2000, Belgium). Polypropylene layers were purchased from Cell Guard. The phenyl-C61 butyric acid methyl ester (PCBM) of >99.5 % purity grade was purchased from Solenne B.V. (The Netherlands).

| Active Material	Specific capacity (mAh g^{-1})	Specific current (A g^{-1})	Reference
Cu_2O	305	–	[1]
V_2O_5	~600	0.15	[2]
$NiCo_2O_4$	694	1	[3]
Fe_3O_4	~1500	0.09	[4]
Si	1870	0.1	[5]
S	~1000	0.1	[6]

Supporting Table S1: Comparative performance of electrodes composed of various active materials embeded inside vertically-aligned CNT forests**.**
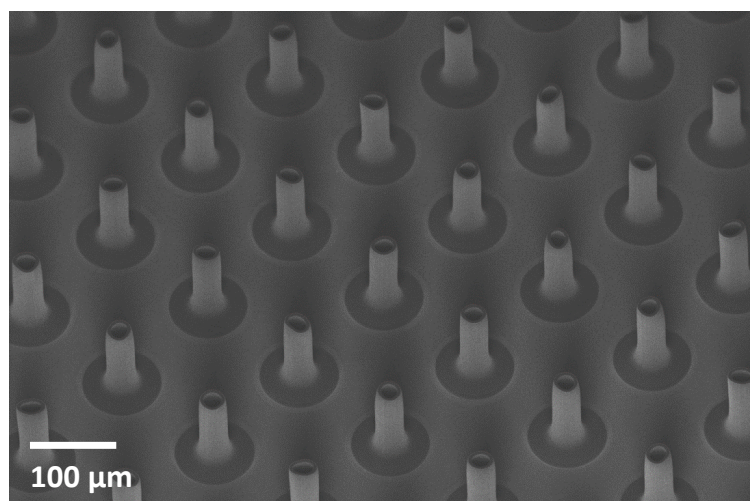
Supporting Figure S1: (Left) SEM image of densified CNT cones on Si - substrate before transfer. The image is taken tilt angle of 35°.
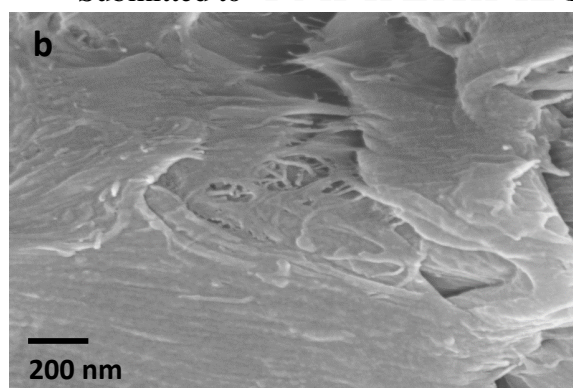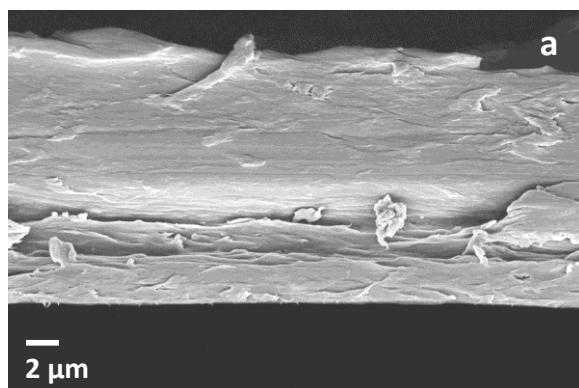
Supporting Figure S2: Cross-sectional SEM images of PCP film. **a,** The cross-sectional image of flexible PCP film shows sea uniform film composition. **b,** The magnified SEM images of PCP film cross-section shows the entangled and connected CNTs.
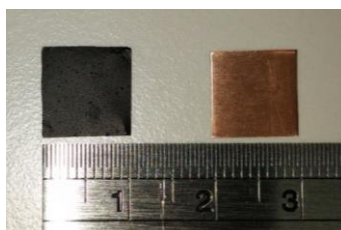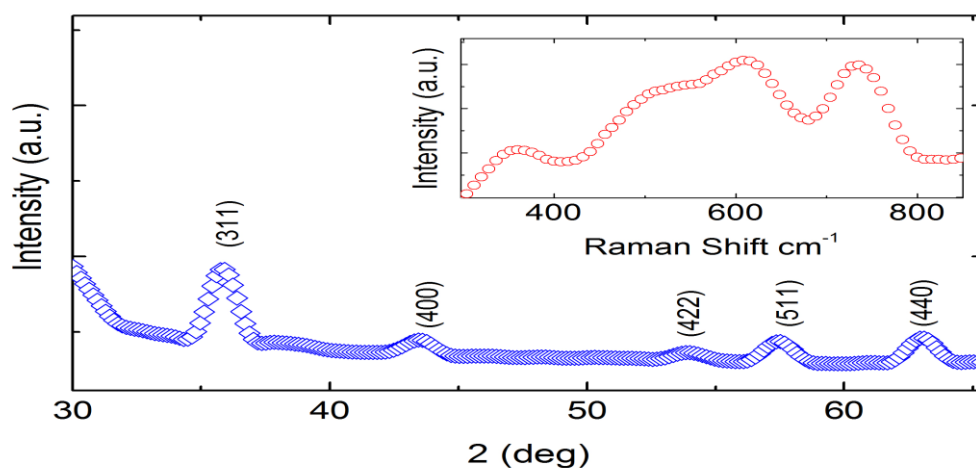

| Film type	PCP	Cu foil
Area	1 x 1 cm^2	1 x 1 cm^2
Average thickness	15 µm	25 µm
Weight	0.0028gm	0.0925gm

Supporting Figure S3: Comparison of weights of an 1 x 1 cm^2 area PCP film and Cu foil
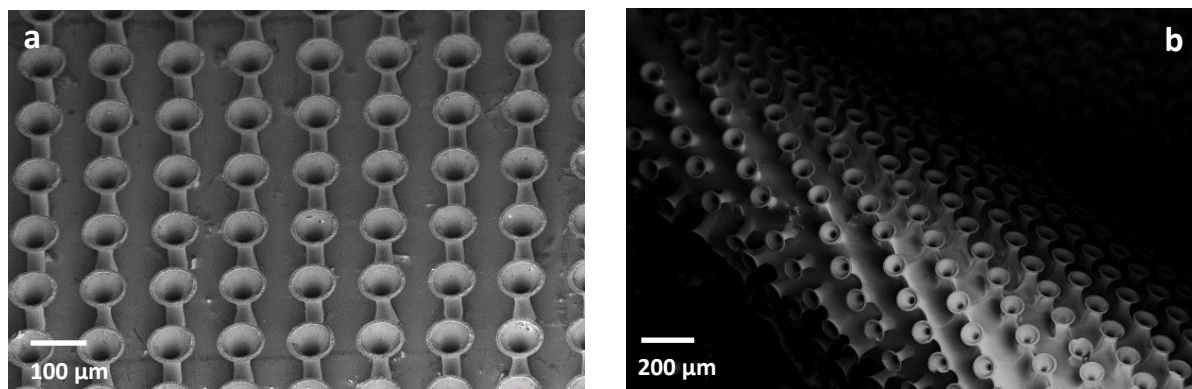
Supporting Figure S4: SEM image of transferred cones, on PCP film, loaded with iron oxide nanocrystals in **(a)** flat and **(b)** bent condition. Image **(a)** is taken at 35° tilt angle.

Supporting Figure S5: Typical thin film X-ray diffraction pattern of iron oxide nanocrystals. The glancing angle thin film X-ray diffraction pattern of iron oxide nanocrystals shows all the characteristic peaks matching consistent with the structure of Fe_2O_3 [7-8] with an inset showing Raman bands.
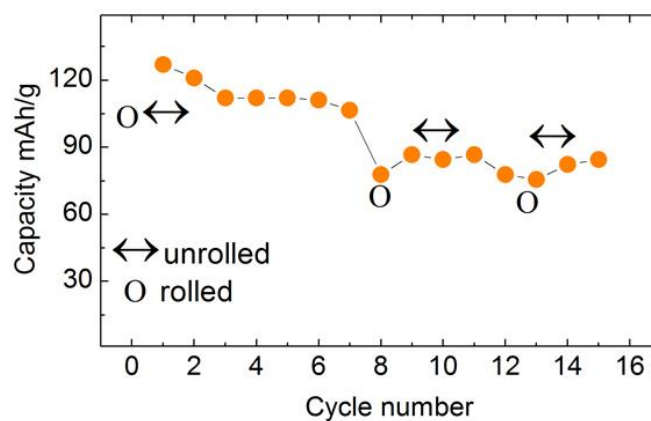
Supporting Figure S6: Cyclic data of full flexible cell at 2C rate while bending and release of cells.

References:

[1]   A. Goyal, A. L. M. Reddy, P. M. Ajayan, *Small* **2011**, 7, 1709.

[2]   W. Lu, A. Goering, L. Qu, L. Dai, *Phys. Chem. Chem. Phys.* **2012**, 14, 12099.

[3]   W. Liu, C. Lu, K. Liang, B. K. Tay, *J. Mater. Chem.* A **2014**, 2, 5100.

[4]   Y. Wu, Y. Wei, J. Wang, K. Jiang, S. Fan, *Nano Lett.* **2013**, 13, 818.

[5]   W. Wang, R. Epur, P. N. Kumta, *Electrochem. commun.* **2011**, 13, 429.

[6]   H. Kim, J. T. Lee, G. Yushin, *J. Power Sources* **2013**, 226, 256.

[7]   W. Kim, C.-Y. Suh, S.-W. Cho, K.-M. Roh, H. Kwon, K. Song, I.-J. Shon, *Talanta* **2012**, 94, 348.

[8]   J. Vidal-Vidal et al, *Colloids and Surfaces A: Physicochemical and Engineering Aspects* **2006**, 288, 1-3, 44.